



KIC 7177553: A QUADRUPLE SYSTEM OF TWO CLOSE BINARIES

H. LEHMANN¹, T. BORKOVITS², S. A. RAPPAPORT³, H. NGO⁴, D. MAWET⁵, SZ. CSIZMADIA⁶, AND E. FORGÁCS-DAJKA⁷¹ Thüringer Landessternwarte Tautenburg, Sternwarte 5, D-07778 Tautenburg, Germany; lehm@tls-tautenburg.de² Baja Astronomical Observatory of Szeged University, H-6500 Baja, Szegedi út, Kt. 766, Hungary; borko@electra.bajaobs.hu³ Massachusetts Institute of Technology, Department of Physics, 77 Massachusetts Avenue, Cambridge, MA 02139-4307, USA; sar@mit.edu⁴ California Institute of Technology, Division of Geological and Planetary Sciences, 1200 E. California Boulevard, MC 150-21, Pasadena, CA 91125, USA; hngo@caltech.edu⁵ California Institute of Technology, Astronomy Dept. MC 249-17, 1200 E. California Boulevard, Pasadena, CA 91125, USA; dmawet@astro.caltech.edu⁶ German Aerospace Center (DLR), Institut für Planeten-forschung, Rutherfordstraße 2, D-12489 Berlin, Germany; szilard.csizmadia@dlr.de⁷ Astronomical Department, Eötvös University, H-1118 Budapest, Pázmány Péter stny. 1/A, Hungary; e.forgacs-dajka@astro.elte.hu

Received 2015 November 20; accepted 2016 January 10; published 2016 February 25

ABSTRACT

KIC 7177553 was observed by the *Kepler* satellite to be an eclipsing eccentric binary star system with an 18-day orbital period. Recently, an eclipse timing study of the *Kepler* binaries has revealed eclipse timing variations (ETVs) in this object with an amplitude of ~ 100 s and an outer period of 529 days. The implied mass of the third body is that of a super-Jupiter, but below the mass of a brown dwarf. We therefore embarked on a radial velocity (RV) study of this binary to determine its system configuration and to check the hypothesis that it hosts a giant planet. From the RV measurements, it became immediately obvious that the same *Kepler* target contains another eccentric binary, this one with a 16.5-day orbital period. Direct imaging using adaptive optics reveals that the two binaries are separated by $0''.4$ (~ 167 AU) and have nearly the same magnitude (to within 2%). The close angular proximity of the two binaries and very similar γ velocities strongly suggest that KIC 7177553 is one of the rare SB4 systems consisting of two eccentric binaries where at least one system is eclipsing. Both systems consist of slowly rotating, nonevolved, solar-like stars of comparable masses. From the orbital separation and the small difference in γ velocity, we infer that the period of the outer orbit most likely lies in the range of 1000–3000 yr. New images taken over the next few years, as well as the high-precision astrometry of the *Gaia* satellite mission, will allow us to set much narrower constraints on the system geometry. Finally, we note that the observed ETVs in the *Kepler* data cannot be produced by the second binary. Further spectroscopic observations on a longer timescale will be required to prove the existence of the massive planet.

Key words: binaries: eclipsing – binaries: spectroscopic – planetary systems – stars: fundamental parameters

1. INTRODUCTION

Most of our knowledge of stellar masses comes from the investigation of binary stars. In particular, eclipsing binaries (EBs) can provide the absolute masses of their components. Precise absolute masses of stars across the whole Hertzsprung–Russell diagram are urgently needed for testing the theories of stellar structure and evolution and, recently, more and more for establishing accurate scaling relations for the pulsation properties of oscillating stars in the rapidly developing field of asteroseismology (e.g., Aerts 2015). This will be especially important for the scaling of measured planet-star mass ratios in such future space projects like *PLATO* (Rauer et al. 2014), where the stellar masses will be asteroseismically determined.

The *Kepler* space telescope mission (Borucki et al. 2011), designed and launched for searching for transiting planets, also delivered light curves of unprecedented photometric quality of a large number of EBs (e.g., Slawson et al. 2011). Among these EBs, multiple systems were also found, including triply eclipsing hierarchical triples such as KOI-126 (Carter et al. 2011a), HD 181068 (Derekas et al. 2011), and KIC 4247791, an SB4 system consisting of two EBs (Lehmann et al. 2012). Such unusual objects (from the observational side) additionally offer the possibility for studying the tidal interaction with the third body or between the binaries in the case of quadruple systems.

EBs in eccentric orbits, on the other hand, allow for the observation of apsidal motion as a probe of stellar interiors (e.g., Claret & Gimenez 1993). Moreover, such types of EBs

are interesting for searching for tidally induced oscillations occurring as high-frequency p -modes in the convective envelopes of the components (e.g., Fuller et al. 2013) or as the result of a resonance between the dynamic tides and one or more free low-frequency g -modes as observed in KOI 54 (Welsh et al. 2011). Tidally induced pulsations allow us to study tidal interaction that impacts the orbital evolution, as well as the interiors of the involved stars.

KIC 7177553 (TYC 3127-167-1) is listed in the catalog Detection of Potential Transit Signals in the First Three Quarters of *Kepler* Mission Data (Tenenbaum et al. 2012) with an orbital period of 18 days. Armstrong et al. (2014) combined the *Kepler* Eclipsing Binary Catalog (Prša et al. 2011; Slawson et al. 2011) with information from the Howell–Everett (HES; Everett et al. 2012), *Kepler* INT (KIS; Greiss et al. 2012), and Two Micron All Sky Survey (2MASS; Skrutskie et al. 2006) photometric surveys to produce a catalog of spectral energy distributions of *Kepler* EBs. They estimate the temperatures of the primary and secondary components of KIC 7177553 to be 5911 ± 360 K and 5714 ± 552 K, respectively, and derive $R_2/R_1 = 0.89 \pm 0.28$ for the ratio of the radii of the components.

In a recent survey of eclipse timing variations (ETVs) of EBs in the original *Kepler* field (Borkovits et al. 2015, B15 hereafter), low-amplitude (~ 90 s) periodic ETVs were found and interpreted as the consequence of dynamical perturbations by a giant planet that revolves around the EB in an eccentric, inclined, 1.45 yr orbit. In order to confirm or reject the

hypothesis of the presence of a nontransiting circumbinary planet in the KIC 7177553 system, we carried out spectroscopic follow-up observations. This article describes the analysis of these observations that led to an unexpected finding, namely, that KIC 7177553 is an SB4 star consisting of two binaries. This fact makes the star an extraordinary object. As a possible quadruple system, its properties are important for our understanding of the formation and evolution of multiple systems (e.g., Reipurth et al. 2014, p. 267) and may be very important for the theory of planet formation in multiple systems (e.g., Di Folco et al. 2014) if one of the binaries in KIC 7177553 hosts the suspected giant planet.

2. SPECTROSCOPIC INVESTIGATION

2.1. Observations and Data Reduction

New spectra were taken in 2015 May to July with the Coude-Echelle spectrograph attached to the 2 m Alfred Jensch Telescope at the Thüringer Landessternwarte Tautenburg. The spectra have a resolving power of 30,000 and cover the wavelength range from 454 to 754 nm. The exposure time was 40 minutes, allowing for the $V = 11^m.5$ star for a typical signal-to-noise ratio (S/N) of the spectra of about 100. The dates of observation are listed in Table 5 in Appendix B, together with the measured radial velocities (RVs; see Section 2.2).

The spectrum reduction was done using standard ESO-MIDAS packages. It included filtering of cosmic rays, bias and straylight subtraction, optimum order extraction, flat fielding using a halogen lamp, normalization to the local continuum, wavelength calibration using a ThAr lamp, and merging of the echelle orders. The spectra were corrected for small instrumental shifts using a larger number of telluric O₂ lines.

2.2. RVs and Orbital Solutions

In a first step, we used the cross-correlation of the observed spectra with an unbroadened synthetic template spectrum based on the 487–567 nm metal line region (redward of H β , where no stronger telluric lines occur) to look for multiple components in the cross-correlation functions (CCFs). The template was calculated with SynthV (Tsymbal 1996) for T_{eff} of 6200 K, based on a model atmosphere calculated with LLmodels (Shulyak et al. 2004). Surprisingly, there were two spectra where we could clearly see four components in the CCFs. In all other spectra, the components were more or less blended and we saw only one to three components.

Next, we used the least-squares deconvolution (LSD; Donati et al. 1997) technique and calculated LSD profiles with the LSD code by Tkachenko et al. (2013), based on the same line mask as we used for our previously mentioned synthetic spectrum. Figure 1 shows the LSD profiles vertically arranged according to the JD of observation. The resolution is distinctly better than that of the CCFs; four components are now seen in the majority of the LSD profiles. The measured RVs are marked, and the calculated orbital curves plotted in Figure 1 show that we could assign all components in all LSD profiles to four different stars located in two different binary systems, $S_{1,2}$ and $S_{3,4}$.

The RVs of the four components, C_1 to C_4 , were determined by fitting the LSD profiles with multiple Gaussians. The mean (internal) errors of the fit were 0.25, 0.36, 0.28, and 0.37 km s⁻¹ for the RVs of C_1 to C_4 , respectively. We used the method of differential corrections (Schlesinger 1910) to

determine the orbits from the RVs. Because of the short time span of the observations, this could be done for the two systems separately, without accounting for any interaction between them or for light-travel-time effects. In the case of $S_{1,2}$, we fixed the orbital period to the value known from the *Kepler* light-curve analysis. The RVs of the four components of KIC 7177553 determined from the multi-Gaussian fit to the LSD profiles are listed in Table 5 in Appendix B.

Figure 2 shows the RVs and orbital curves folded with the orbital periods. Table 1 lists the derived orbital parameters. The times of observation of all spectra are based on UTC. To be consistent with the *Kepler* DCT time scale and the results listed in Table 3, we added 68 s to the calculated times of periastron passage T .

The O–C residuals after subtracting the orbital solutions from the RVs are shown in Figure 3, together with straight lines resulting from a linear regression using 2σ -clipping to reject outliers. The slopes of the regression lines are -5.3 ± 1.5 , -6.9 ± 2.0 , 1.6 ± 1.8 , and 2.6 ± 1.5 km s⁻¹ yr⁻¹ for C_1 to C_4 , respectively. These slopes describe a change in the systemic velocities of the two binaries or additional RV components of the single objects not included in our Keplerian orbital solutions. They are different from zero by 3.5 times the 1σ error bars for C_1 and C_2 but much less than or not significantly different from zero for C_3 and C_4 . There are no outliers anymore when using 3σ -clipping for the linear regression, however, and all slopes turn out to be nonsignificant.

The typical accuracy in RV that we can reach with our spectrograph and reduction methods (without using an iodine cell) for a single-lined, solar-type star with such sharp lines and spectra with S/N of 100 is of about 150 m s⁻¹. The rms as listed in Table 1 is distinctly higher. To check for periodic signals possibly hidden in the O–C residuals, we performed a frequency search using the Period04 program (Lenz & Breger 2005). It did not reveal any periodicity in the residuals of any of the components. We assume that the higher rms results from the fact that we are dealing with an SB4 star using multi-Gaussian fits to disentangle the blended components in the LSD profiles and to derive the RVs and assume that the listed rms stands for the measurement errors.

2.3. Spectrum Decomposition

We used the KOREL program (Hadrava 1995, 2006) provided by the VO-KOREL⁸ web service (Škoda & Hadrava 2010) for decomposing the spectra. Allowing for timely variable line strengths of all four components, we got smooth decomposed spectra with only slight undulations in the single continua as they are typical for Fourier-transform-based methods of spectral disentangling (see, e.g., Pavlovski & Hensberge 2010). These undulations were removed by comparing the KOREL output spectra with the mean composite spectrum and applying continuum corrections based on spline fits.

The resulting orbital parameters are listed and compared to those obtained in Section 2.2 in Table 1. The Fourier-transform-based KOREL program does not deliver the systemic velocity and also does not provide the errors of the derived parameters. The parameter errors were calculated by solving the orbits with the method of differential corrections

⁸ <https://stelweb.asu.cas.cz/vo-korel/>

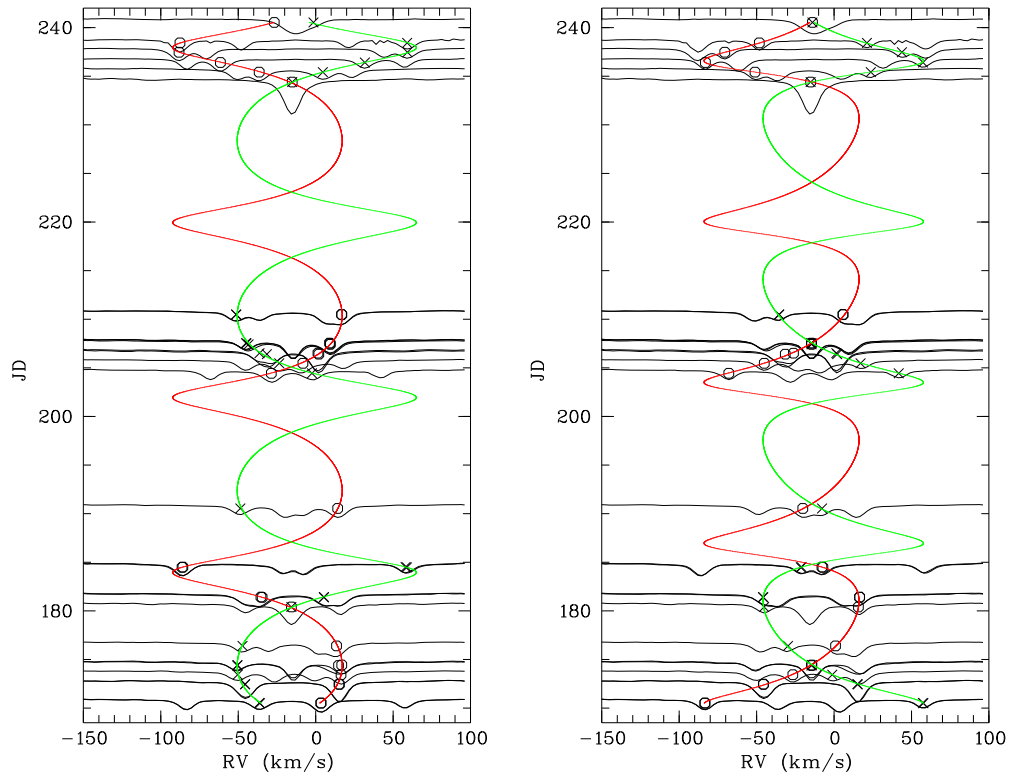


Figure 1. LSD profiles calculated from the 29 spectra, vertically arranged according to the JD (2,457,000+) of observation. Measured RVs are marked by open circles and crosses, in the left panel for components C_1 and C_2 and in the right panel for C_3 and C_4 , respectively. The red and green curves illustrate the corresponding, calculated orbital solutions.

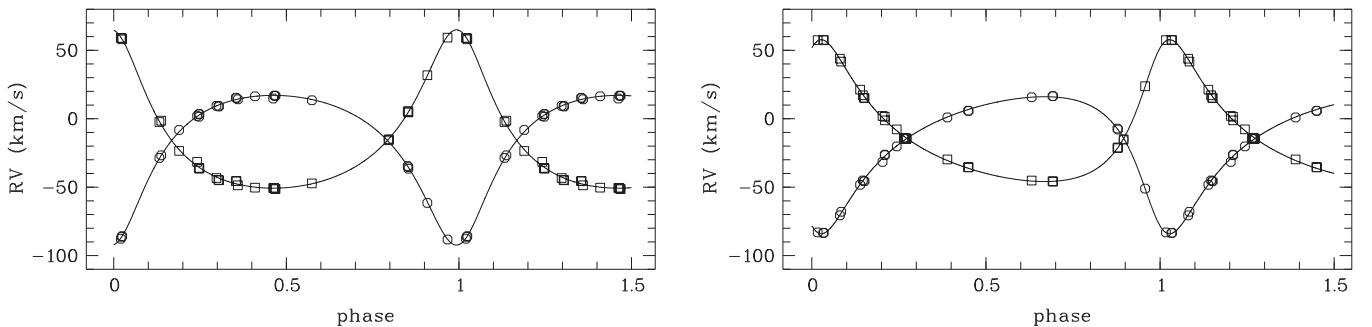


Figure 2. RVs and calculated orbital curves folded with the orbital periods. Left: C_1 (open circles) and C_2 (open squares). Right: C_3 (open circles) and C_4 (open squares). Phase zero corresponds to the time of periastron passage.

using the orbital parameters and line shifts delivered by the KOREL program as input. Comparing the results with those obtained from the LSD-based RVs, we see that there is agreement within the 1σ error bars. The rms of the residuals of the KOREL solutions for the single components is distinctly lower, however. The last row lists the projected masses calculated from the spectroscopic mass functions. It can be seen that the minimum masses derived for system $S_{3,4}$ are distinctly lower than those of $S_{1,2}$, which implies different viewing angles for the two systems.

2.4. Spectrum Analysis

We used the spectrum-synthesis-based method as described in Lehmann et al. (2011) to analyze the decomposed spectra of the four components. The method compares the observed spectra with synthetic ones using a huge grid in stellar parameters. A description of an advanced version of the

program can also be found in Tkachenko (2015). Synthetic spectra are computed with SynthV (Tsymbal 1996) based on atmosphere models calculated with LLmodels (Shulyak et al. 2004). Both programs consider plane-parallel atmospheres and work in the LTE regime. Atomic and molecular data were taken from the VALD⁹ database (Kupka et al. 2000).

One main problem in the spectrum analysis of multiple systems is that programs for spectral disentangling like KOREL deliver the decomposed spectra normalized to the common continuum of all involved stars. To be able to renormalize the spectra to the continua of the single stars, we have to know the continuum flux ratios between the stars in the considered wavelength range. These flux ratios can be obtained during the spectrum analysis itself from a least-squares fit between the observed and the synthetic spectra, as we show in

⁹ <http://vald.astro.univie.ac.at/~vald/php/vald.php>

Table 1
Orbital Solutions Obtained from Multi-Gaussian Fits of the LSD Profiles and with KOREL

Parameter	LSD				KOREL			
	$S_{1,2}$		$S_{3,4}$		$S_{1,2}$		$S_{3,4}$	
P (day)	17.996467(17)		16.5416(70)		17.996467(17)		16.5490(38)	
e	0.3984(31)		0.4437(35)		0.4008(17)		0.4421(12)	
ω ($^\circ$)	6.51(63)		332.30(75)		6.76(42)		331.17(27)	
T (BJD)	2 457 184.067(27)		2 457 186.505(34)		2 457 184.039(21)		2 457 186.457(13)	
q	0.9457(71)		0.9664(78)		0.9359(36)		0.9612(27)	
	C_1	C_2	C_3	C_4	C_1	C_2	C_3	C_4
K (km s $^{-1}$)	54.70(26)	57.84(34)	50.06(30)	51.80(28)	54.94(17)	58.70(13)	50.148(94)	52.17(11)
γ (km s $^{-1}$)	−15.98(17)	−15.77(22)	−14.30(19)	−14.43(18)
rms (km s $^{-1}$)	0.873	1.17	0.936	0.871	0.45	0.35	0.26	0.30
M_{\min} (M_\odot)	1.054(14)	0.997(12)	0.663(9)	0.641(9)	1.0871(64)	1.0174(71)	0.6758(34)	0.6496(31)

Note. The table lists period P and orbital elements (eccentricity e , argument of periastron ω , time of periastron passage T , and mass ratio q) of the two systems, and the RV semiamplitudes K and individual systemic velocities γ . Errors are given in units of the last two digits in parentheses. The last two rows list the rms of the residuals after subtracting the orbital solution from the RVs and the projected masses calculated from the spectroscopic mass function.

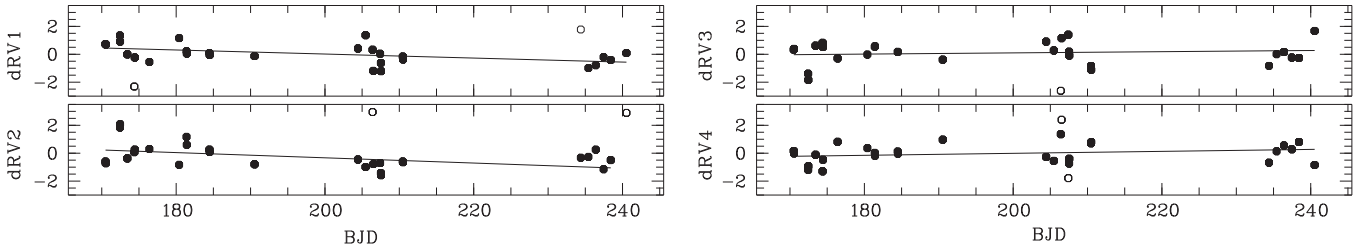


Figure 3. O–C values in km s $^{-1}$ vs. BJD (2,457,000+) for components C_1 to C_4 . The straight lines result from a linear regression calculated from all RVs shown by filled circles. Outliers are indicated by open circles.

Appendix A. We extended our program accordingly and tested the modified version successfully on synthetic spectra.

The analysis is based on the wavelength interval 455–567 nm that includes H β and is almost free of telluric contributions. It was performed using four grids of atmospheric parameters for the four stars. Each grid consists of (step widths in parentheses) T_{eff} (100 K), $\log g$ (0.1 dex), v_{turb} (1 km s $^{-1}$), $v \sin i$ (1 km s $^{-1}$), and scaled solar abundances [M/H] (0.1 dex). The analysis includes all four spectra simultaneously, which are coupled via the flux ratios. To obtain the optimum flux ratios and renormalize the spectra, we solved Equation (19) (see Appendix A) for each combination of atmospheric parameters.

The results of the analysis are listed in Table 2. The given errors were obtained from χ^2 statistics as described in Lehmann et al. (2011). They were calculated from the full grid in all parameters per star, i.e., the errors include all interdependencies between the different parameters of one star. We did not have enough computer power to include the interdependencies between the parameters of different stars that interfere in the simultaneous analysis via the flux ratios, however.

3. LIGHT-CURVE ANALYSIS

3.1. Long-cadence (LC) Data

For the photometric light-curve analysis we downloaded the preprocessed, full Q0–Q17 *Kepler* LC data series from the

Table 2
Atmospheric Parameters of the Four Stars

Parameter	C_1	C_2	C_3	C_4
[M/H] (dex)	0.00(11)	−0.10(13)	−0.12(13)	−0.12(13)
T_{eff} (K)	5800(130)	5700(150)	5600(150)	5600(140)
$\log g$ (c.g.s.)	4.75(38)	4.55(40)	4.63(38)	4.59(35)
v_{turb} (km s $^{-1}$)	1.76(60)	1.23(63)	1.29(65)	1.02(59)
$v \sin i$ (km s $^{-1}$)	1.3(4.2)	3.9(3.7)	5.8(3.6)	2.5(4.2)
f	0.30	0.23	0.24	0.23

Note. Errors are given in parentheses, in units of the last digits. f is the continuum flux ratio of the components.

Villanova site¹⁰ of the *Kepler* Eclipsing Binary Catalog (Prša et al. 2011; Slawson et al. 2011; Matijević et al. 2012). Note that the same data set was used for the ETV analysis of KIC 7177553, which is described in detail in B15. This ~1470-day-long light curve was folded, binned, and averaged for the analysis. The out-of-eclipse sections were binned and averaged equally into 0^p002 phase-length cells, while for the narrow primary and secondary eclipses, i.e., in the ranges of $\phi_{\text{pri}} = [-0^p005; 0^p005]$ and $\phi_{\text{sec}} = [0^p737; 0^p747]$, a four times denser binning and averaging was applied. The resulting folded light curve is shown in Figure 4.

The light-curve analysis was carried out with the LIGHT-CURVEFACTORY program (Borkovits et al. 2013, 2014). The primary fitted parameters were the initial epoch T_0 , orbital eccentricity (e), argument of periastron (ω), inclination (i), fractional radii of the stars ($r_{1,2} = R_{1,2}/a$), effective

¹⁰ <http://keplerebs.villanova.edu/>

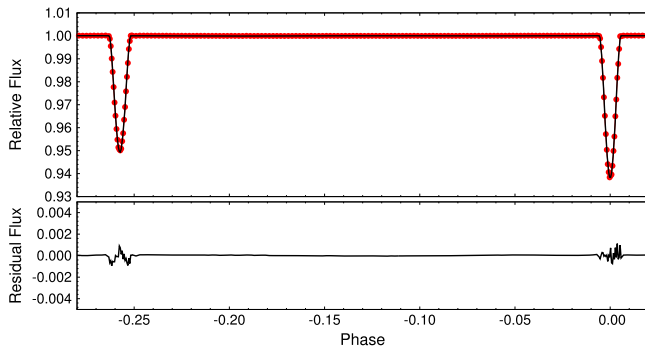


Figure 4. *Kepler* light curve of KIC 7177553. Upper panel: folded, binned, averaged light curve (red circles), together with the model solution (black line). Lower panel: residual light curve.

temperature of the secondary (T_2), luminosity of the primary (L_1), and the amount of third light (l_3). The effective temperature of the primary (T_1) and the mass ratio (q), as well as the chemical abundances, were taken from the spectroscopic solution. The other atmospheric parameters, such as limb darkening (LD), gravity brightening coefficients, and bolometric albedo, were set in accordance with the spectroscopic results and also kept fixed. For LD, the logarithmic law (Klinglesmith & Sobieski 1970) was applied, and the coefficients were calculated according to the passband-dependent precomputed tables¹¹ of the PHOEBE team (Prša & Zwitter 2005; Prša et al. 2011), which are based on the tables of Castelli & Kurucz (2004). Table 3 lists the parameters obtained from the light-curve solution, together with some other quantities that can be calculated by combining the photometric and spectroscopic results. Figure 4 compares our model solution with the observed light curve.

The out-of-eclipse behavior of the light curve merits some further discussion. The primary and secondary eclipse depths are 60,000 and 50,000 ppm, respectively. By contrast, all of the physical out-of-eclipse effects, both expected and observed, are $\lesssim 60$ ppm. From a simple Fourier series we found several residual sinusoidal features in the folded light curve at a number of frequencies near to higher harmonics of the orbit. The amplitudes of these sinusoids ranged from 10 to 37 ppm. A comparison with the amplitudes expected from different physical effects gives the following picture, where our estimations are based on Carter et al. (2011b): the asymmetric ellipsoidal light variation amplitudes are ~ 5 and ~ 60 ppm at apastron and periastron, respectively. The Doppler boosting (DB) effect has a peak value of ~ 300 ppm for each one of the stars, but their velocities are 180° out of phase. Since the luminosity of the two stars differs by only $\sim 3\%$ (see Table 3), this leads to a net DB amplitude of not more than 10 ppm. The illumination (or reflection effect) ranges from ~ 4 ppm at apastron to ~ 30 ppm at periastron, after taking into account that the first-order terms at the orbital frequency essentially cancel because of the twin nature of the two stars.

Finally, we allowed the *amplitudes* of these sinusoids to be free parameters in the fitting procedure in a purely mathematical way, together with the physical modeling of the well-known ellipsoidal and other effects. These terms have only a minor influence on the light-curve solution, however, which is

Table 3
Orbital and Stellar Parameters of the $S_{1,2}$ System

Orbital Parameters and Third-light Contribution		
Parameter	Value	
P_{orb} (day)	17.996467 ± 0.000017	
T	$5\,690.213 \pm 0.012$	
T_{MINI}	$4\,954.545842 \pm 0.00020$	
a (R_{\odot})	36.76 ± 0.15	
e	0.3915 ± 0.0010	
ω ($^{\circ}$)	3.298 ± 0.061	
i ($^{\circ}$)	87.679 ± 0.055	
q_{spec}	0.9457 ± 0.0071	
l_3	0.453 ± 0.043	
Fixed Coefficients and Deduced Stellar Parameters		
Parameter	C_1	C_2
x_{bol}	0.694	0.695
y_{bol}	0.160	0.159
x_{kep}	0.666	0.670
y_{kep}	0.192	0.192
A	0.5	0.5
β	0.32	0.32
r	0.02556 ± 0.00010	0.02561 ± 0.00010
M (M_{\odot})	1.043 ± 0.014	0.986 ± 0.015
R (R_{\odot})	0.940 ± 0.005	0.941 ± 0.005
T_{eff} (K)	5800 ± 130	5740 ± 140
L (L_{\odot})	0.88 ± 0.08	0.85 ± 0.08
$\log g$ (dex)	4.517 ± 0.008	4.491 ± 0.008

Note. T and T_{MINI} are BJD 2,450,000+, l_3 is the photometric third-light contribution, x_{bol} , y_{bol} are the linear and logarithmic bolometric LD coefficients, x_{kep} , y_{kep} are the linear and logarithmic LD coefficients for the *Kepler* passband, A is the coefficient for the bolometric albedo, β is the gravitational brightening exponent, and r is the fractional radius.

mainly based on the eclipses whose amplitudes are three orders of magnitude larger.

As one can see from Tables 2 and 3, the photometric solution and especially the third-light contribution to the *Kepler* light curve are in good agreement with the spectroscopic results. It confirms that the spectrum decomposition and our derivation of spectroscopic flux ratios, both applied to an SB4 star for the first time, give quite reliable results.

3.2. Short-cadence (SC) Data

The combined spectroscopic-photometric analysis revealed that the KIC 7177553 system consists of four very similar solar-like main-sequence stars, and thus we might expect to find solar-like oscillations in the *Kepler* light curve. The frequency of maximum power, ν_{max} , can be estimated using the scaling relation

$$\nu_{\text{max}} = \frac{M/M_\odot (T_{\text{eff}}/T_{\text{eff},\odot})^{3.5}}{L/L_\odot} \nu_{\text{max},\odot} \quad (1)$$

(Brown et al. 1991). From the values given in Tables 2 and 3 we estimate that ν_{max} should lie in the range 2650–3700 μHz , or 230–320 day^{-1} , far beyond the Nyquist frequency of the LC data of 24.469 day^{-1} . Unfortunately, only one SC run spanning 30 days exists, having a Nyquist frequency of greater than 700 day^{-1} . We clipped off the four eclipses that appear in this segment and ran it through a high-pass filter with a cutoff

¹¹ <http://phoebe-project.org/1.0/?q=node/110>

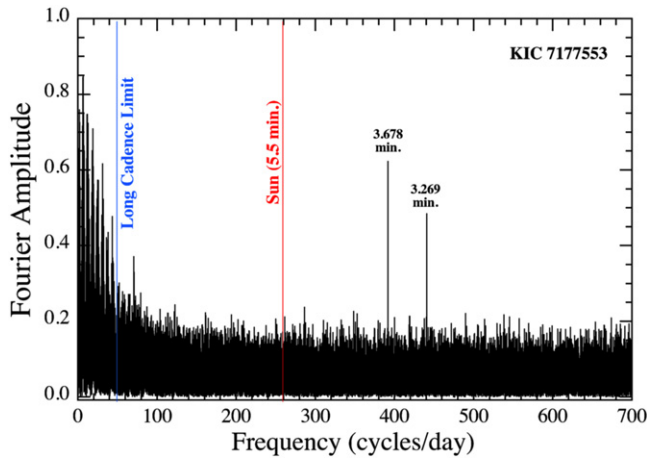


Figure 5. Periodogram of the *Kepler* SC data of KIC 7177553.

frequency of 0.5 day^{-1} . Figure 5 shows the result of a Fourier-transform-based frequency search. No hint to solar-like oscillations could be found. Only two isolated peaks corresponding to periods of 3.678 and 3.269 minutes appear. These are known artifacts of the *Kepler* SC light curves representing the 7th and 8th harmonics of the inverse of the LC sampling of 29.4244 minutes (see, e.g., Gilliland et al. 2010). No further prominent peaks or typical bump in the periodogram could be detected.

Solar-like oscillations have been found for most of the investigated solar-type and red subgiant and giant stars (e.g., White et al. 2011; Chaplin & Miglio 2013), and, at first sight, the lack of such finding in our data might seem surprising. There is a simple explanation, however. The pulsation amplitude strongly decreases with increasing ν_{max} (Campante et al. 2014), making solar-like pulsations less detectable for stars of higher $\log(g)$ (or easier to detect for giant than for main-sequence stars). The detectability, on the other hand, depends on the noise background, the apparent brightness of the star, and the length of the observation cycle. Chaplin et al. (2011) performed an investigation of the detectability of oscillations in solar-type stars observed by *Kepler*. From their Figure 6 it can easily be seen that our object is too faint (or the observing period too short), and the detection probability based on one SC run is close to zero.

4. DIRECT IMAGING

An examination of the UKIRT *J*-band image of KIC 7177553 showed only a single stellar image. From the lack of any elongation of the image, we concluded that the angular separation of the two binaries is $\lesssim 0''.5$. To obtain better constraints, we imaged the object on 2015 October 26 UT with the NIRC2 instrument (PI: Keith Matthews) on Keck II using K_s -band (central wavelength $2.146 \mu\text{m}$) natural guide star imaging with the narrow camera setting ($10 \text{ mas pixel}^{-1}$). To avoid NIRC2's noisier lower left quadrant, we used a three-point dither pattern. We obtained six images with a total on-sky integration time of 30 s. We used dome flat fields and dark frames to calibrate the images and also to find and remove image artifacts.

The resultant stacked AO image is shown in Figure 6, where we see two essentially twin images separated by $0''.4$. For each calibrated frame, we fit a two-peak point-spread function (PSF)

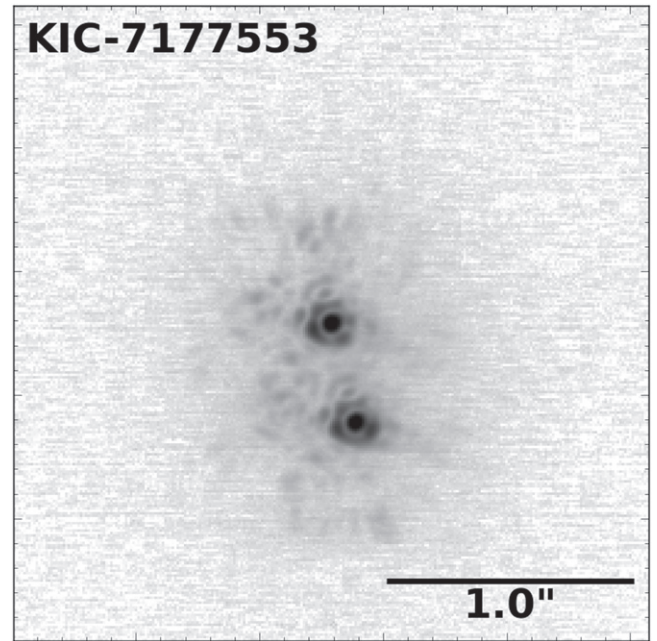


Figure 6. Stacked image produced from the six NIRC2 frames showing the two well-separated binaries of KIC 7177553. The intensity is displayed on a logarithmic scale.

to measure the flux ratio and on-sky separations. We chose to model the PSF as a Moffat function with a Gaussian component. The best-fit PSF model was found over a circular area with a radius of 10 pixels around each star (the FWHM of the PSF was about 5 pixels). More details of the method can be found in Ngo et al. (2015).

For each image, we also computed the flux ratio by integrating the best-fit PSF model over the same circular area. When computing the separation and position angle, we applied the astrometric corrections from Yelda et al. (2010) to account for the NIRC2 array's distortion and rotation. Finally, we report the mean value and the standard error on the mean as our measured values of flux ratio (primary to secondary), separation, and position angle of the system, which are 1.018 ± 0.005 , $410.4 \pm 1.5 \text{ mas}$, and $193.6 \pm 0.2^\circ \text{ E of N}$, respectively.

5. CONFIGURATION OF THE QUADRUPLE

As was mentioned in the introduction, the B15 study found low-amplitude, $\sim 1.45 \text{ yr}$ period ETVs in KIC 7177553, which they interpreted as the perturbations by a giant planet. The short period of 1.45 yr, together with a total mass of both binaries of about $4 M_\odot$ estimated from the spectrum analysis, would yield a separation of the two systems of only 2 AU and dynamically forced ETVs of the order of 1.5 hr (see Equation (11) in B15). It is evident from the results of direct imaging that the 16.5-day-period binary located in such a distant system and separated by $\sim 0''.4$ cannot produce such a signal.

We also conclude that there is no evidence for either light-travel-time effect or dynamical perturbations caused by the 16.5-day binary in the $\sim 4 \text{ yr}$ long *Kepler* observations of KIC 7177553. This fact does not eliminate the possibility that the two binaries form a quadruple system, of course, but indicates that the period of the orbital revolution of the two binaries around each other must exceed at least a few decades.

Based on the quite reasonable approximation that all four stars are of spectral type G2 V and taking the (total) apparent magnitude, $m_V = 11.629 \pm 0.020$, and color index, $B - V = 0.741 \pm 0.028$, from Everett et al. (2012) and $M_V = 4.82 \pm 0.01$, $(B - V)_0 = 0.650 \pm 0.01$ from the solar values as given in Cox (2000), we estimate that the distance to this quadruple system is $D = 406 \pm 10$ pc. In that case, the projected physical separation is $s = 167 \pm 5$ AU and the orbital period P must be larger than 1000 yr (note that we assigned to the errors of D and s twice the values that would follow from error propagation, accounting for the approximation that all four stars have identical properties).

Because we measure only two instantaneous quantities related to the outer orbit, s , the separation of the two components, and $\Delta\gamma$, the relative RV between the two binaries (or difference in γ -velocities), we obviously cannot uniquely determine the orbital properties of the quadruple system. However, we can set some quite meaningful constraints on the outer orbit.

Starting with the simpler circular orbit case, we can show that

$$s = a\sqrt{\cos^2 i + \cos^2 \phi \sin^2 i} \quad (2)$$

$$\Delta\gamma = \sqrt{\frac{GM}{a}} \cos \phi \sin i, \quad (3)$$

where a is the orbital separation, ϕ the orbital phase, i the orbital inclination angle, and M the total system mass. The unknown orbital phase can be eliminated to find a cubic expression for the orbital separation:

$$a^3 \left(\frac{\Delta\gamma^2}{GM} \right) + a^2 \cos^2 i - s^2 = 0. \quad (4)$$

In spite of the fact that we do not know the orbital inclination angle, i , we can still produce a probability distribution for a (and hence P_{orb}) via a Monte Carlo approach. For each realization of the system we choose a random inclination angle with respect to an isotropic set of orientations of the orbital angular momentum vector. In addition, because there are uncertainties in the determination of s (accruing from the uncertainty in the distance) and in $\Delta\gamma$ (see Table 1), we also choose specific realizations for these two quantities using Gaussian random errors. In particular, we take $s = 167 \pm 5$ AU and $\Delta\gamma = 1.5 \pm 0.28$ km s⁻¹, both as 1σ uncertainties. We then solve Equation (3) for a , and we also record the corresponding value of i . If any inclination leads to a nonphysical solution of Equation (3), we discard it, including the value of i that led to it. We repeat this process some 10^8 times to produce our distributions.

In a similar fashion, for each realization of the system, we can also compute the expected sky motion of the vector connecting the two stars. In particular, we find

$$\frac{\dot{s}}{s} = -\frac{2\pi}{P_{\text{orb}}} \left(\frac{a}{s} \right)^2 \sin \phi \cos \phi \sin^2 i \quad (5)$$

$$\dot{\Theta} = \frac{2\pi}{P_{\text{orb}}} \left(\frac{a}{s} \right)^2 \cos i, \quad (6)$$

where Θ is commonly referred to as the “position angle” on the sky.

We can also find a P_{orb} distribution for the eccentric orbit case. We do this by deriving equations analogous to

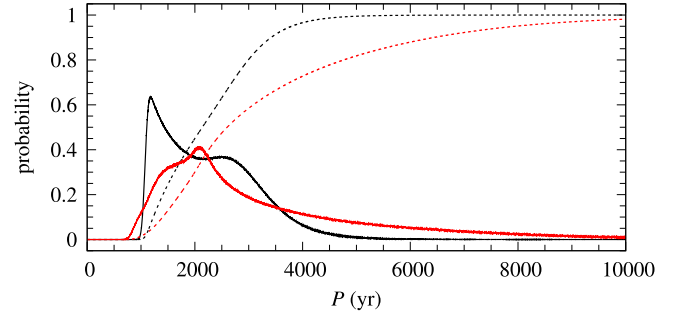


Figure 7. PDFs (solid lines) and corresponding cumulative probabilities (dashed lines) for circular (black) and eccentric (red) orbits. For a better visualization, we scaled the PDFs by a factor of 100.

Equations (1) and (2) for the circular orbit case, except that we now must introduce two more unknown quantities, namely, e , the outer eccentricity, and ω , the corresponding longitude of periastron. These expressions can be written schematically as

$$s = a\sqrt{f_1(e, i, \omega, E) + f_2(e, i, \omega, E)} \quad (7)$$

$$\Delta\gamma = \sqrt{\frac{GM}{a}} g(e, i, \omega, E), \quad (8)$$

where E is the eccentric anomaly at the time of our measurements. The explicit expressions for f and g are

$$f_1 = [(\cos E - e) \cos \omega - \sqrt{1 - e^2} \sin E \sin \omega]^2 \quad (9)$$

$$f_2 = [\sqrt{1 - e^2} \sin E \cos \omega + (\cos E - e) \sin \omega]^2 \cos^2 i \quad (10)$$

$$g = \frac{(\sqrt{1 - e^2} \cos E \cos \omega - \sin E \sin \omega) \sin i}{1 - e \cos E}. \quad (11)$$

As we did for the circular orbit case, we choose i from an isotropic distribution and choose specific values for both s and $\Delta\gamma$ based on their measured values and assumed Gaussian-distributed uncertainties. We choose the longitude of periastron, ω , from a uniform distribution, as is quite reasonable.

Finally, we need to choose a representative value of the outer eccentricity to close the equations. For this, we utilized the distribution of eccentricities of the outer orbits of 222 hierarchical triple systems found in the *Kepler* field (B15). This distribution has a maximum at about $e = 0.35$. Although the outer orbit of KIC 7177553 is two orders of magnitude larger than is typical for the *Kepler* triples, we consider the derived distribution as a plausible proxy for quadruple systems consisting of two widely separated close binaries. Therefore, we chose $e = 0.35$ as a statistically representative value for the eccentricity in KIC 7177553. Equations (6) and (7) are then solved numerically for a by eliminating E .

Figures 7–9 show the probability density functions (PDFs) resulting from 10^8 Monte Carlo trials, together with the corresponding cumulative probability distributions. We obtain highly asymmetric PDFs with maxima at $P = 1180$ yr, $\dot{s} = 1.38$ mas yr⁻¹, and $\dot{\Theta} = 0^\circ 28$ yr⁻¹ for circular orbits. Allowing for noncircular orbits, the peak in the PDF is shifted to $P = 2060$ yr and the tail of the PDF extends to more than 10,000 yr. Table 4 lists the confidence intervals obtained from the cumulative probability distributions. Here 1σ is a formal designation corresponding to 67.27% probability as in the case of a normal distribution.

Table 4
1 σ Confidence Intervals

Parameter	Value
P	1660–2640 yr
\dot{s}	0.67–1.21 mas yr ^{−1}
$\dot{\Theta}$	0°14–0°25 yr ^{−1}
P_e	2070–3550 yr

Note. Derived from the cumulative probability distributions for circular orbits (P , \dot{s} , $\dot{\Theta}$) and for an orbit with $e = 0.35$ (P_e).

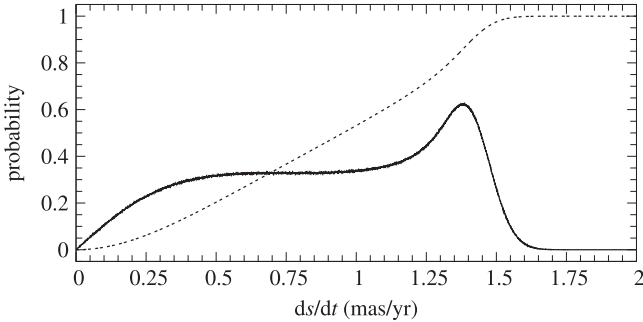


Figure 8. Same as Figure 7 but for \dot{s} and circular orbits. The PDF was scaled by a factor of 0.5.

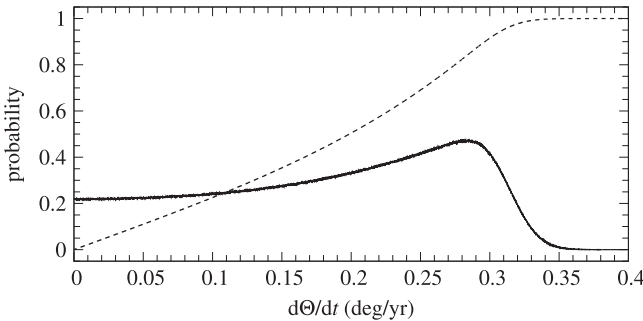


Figure 9. Same as Figure 7 but for $\dot{\Theta}$ and circular orbits. The PDF was scaled by a factor of 0.1.

We also know from the EB light-curve solution of the 18-day binary that its orbital inclination with respect to the observer’s line of sight is $i_1 = 87^\circ.68 \pm 0^\circ.06$. If the constituent stars in the two binaries are very similar, as their spectra suggest, then the orbital inclination angle of the 16.5-day binary must be close to 60° in order for the mass function to yield masses close to $1 M_\odot$. This implies that the two orbital planes must be tilted with respect to each other by at least $\sim 25^\circ$ – 30° .

6. CONCLUSIONS

The analysis of the RV curves derived from the LSD profiles revealed the SB4 nature of the KIC 7177553 system and allowed us to calculate precise orbital solutions for the two underlying binaries. The orbital parameters derived from the LSD profiles are consistent with those delivered by the KOREL program. We find two eccentric systems having only slightly different binary periods and consisting of components of almost the same masses. The systemic velocities of both systems differ by only 1.5 km s^{-1} .

The analysis of the decomposed spectra showed that all four stars are of comparable spectral type. The errors in the derived

atmospheric parameters are relatively large, however. The reason is that we had to solve for the flux ratios between the stars as well, and thus the number of the degrees of freedom in the combined analysis is high. In the result, all atmospheric parameters agree within 1σ of the error bars. What we can say is that all components of the two systems are main-sequence G-type stars showing abundances close to solar, i.e., we are dealing with four slowly rotating, unevolved, solar-like stars. Component C_1 has a slightly higher mass and shows the higher continuum flux. It seems likely that it also has a higher temperature, i.e., that the obtained difference in T_{eff} compared to the other three stars (Table 2) is significant. The EB light-curve analysis of the *Kepler* long-cadence photometry confirmed the spectroscopic results.

KIC 7177553 most likely belongs to the rare known SB4 quadruple systems consisting of two gravitationally bound binaries. This assumption is strongly supported by the similar spectral types and apparent magnitudes of the two binaries, as well as by their small angular separation and similar γ velocities. In particular, several AO surveys (see, e.g., Bowler et al. 2015; Ngo et al. 2015) show that for nearby objects (up to few hundred parsecs) almost every pair of stars that is this bright and this closely separated has been shown to be physically associated. But as is the case of KIC 4247791 (Lehmann et al. 2012), the time span of actual spectroscopic observations is too short to search for any gravitational interaction between the two binaries, and we neglected such effects in the calculation of their individual binary orbits.

The analysis of the O–C values from fitting the RV curves showed that there are no significant changes in the systemic velocities during the time span of the spectroscopic observations. Only when defining outliers based on a 2σ -clipping did we observe a decrease of the systemic γ -velocity of the 18-day binary. Though it is not accompanied by a corresponding increase of the same order of the γ -velocity of the other binary, it could be related to a third body in the 18-day binary such as the giant planet we are searching for. In a similar way, the analysis of the ETVs of the eclipsing pair that is described in B15 neither proves nor refutes the probable gravitationally bounded quadruple system scenario, but indicates a possible nontransiting circumbinary planet companion around the 18-day eclipsing pair of KIC 7177553.

The outer orbital period of the quadruple system must be longer than 1000 yr, and the corresponding probability distribution peaks at about 1200 yr for circular and at about 2000 yr when assuming eccentric orbits with $e = 0.35$. Thus, no orbital RV variations can be measured from spectroscopy in the next decade. Further spectroscopic observations are valuable to extend the search for the hypothetical planetary companion, however.

The proper motion of KIC 7177553 in R.A. cos(Dec) and Dec is given in the Tycho-2 catalog (Høg et al. 2000) as 6.6 and 14.5 mas yr^{-1} , respectively. This is distinctly larger than the expected change of the projected separation of the two binaries on the sky per year, \dot{s} , and future measurements will show whether both binaries have the same proper motion. But also \dot{s} , as well as a change of the position angle, $\dot{\Theta}$, can be measured from speckle interferometry or direct imaging using adaptive optics in the next few years. The observations with the Keck NIRC2 camera, for example, yield an accuracy of about 1.5 mas in radial separation and about 0.2 in position angle, which could be sufficient for a secure measurement of \dot{s} and $\dot{\Theta}$.

Table 5
Radial Velocities Measured for the Four Components of KIC 717755

BJD	S/N	RV ₁	σ_1	RV ₂	σ_2	RV ₃	σ_3	RV ₄	σ_4
2,457,170.502322	82	3.278	0.105	−35.959	0.144	−83.492	0.123	57.663	0.148
2,457,170.532774	116	3.525	0.101	−36.369	0.139	−83.282	0.123	57.326	0.144
2,457,172.437936	104	15.358	0.104	−45.638	0.129	−45.638	0.129	15.358	0.104
2,457,172.466640	99	15.025	0.100	−45.516	0.136	−45.516	0.136	15.025	0.100
2,457,173.433937	111	16.382	0.139	−50.365	0.200	−26.624	0.149	−1.158	0.177
2,457,174.380735	81	14.755	0.196	−50.641	0.374	−14.586	0.172	−14.586	0.172
2,457,174.432658	116	16.837	0.177	−50.461	0.258	−14.332	0.116	−14.332	0.116
2,457,176.399426	80	13.496	0.159	−47.224	0.208	0.959	0.203	−29.714	0.188
2,457,180.403582	101	−15.686	0.099	−15.686	0.099	15.734	0.175	−45.171	0.196
2,457,181.394521	73	−34.550	0.269	5.267	0.325	16.495	0.320	−45.715	0.320
2,457,181.423469	105	−35.344	0.264	5.359	0.304	16.516	0.268	−45.907	0.286
2,457,184.475914	133	−86.269	0.121	58.888	0.177	−7.206	0.167	−21.470	0.143
2,457,184.505151	113	−85.764	0.121	58.062	0.177	−7.841	0.175	−20.992	0.152
2,457,190.536552	125	14.216	0.129	−48.633	0.182	−20.204	0.154	−7.757	0.188
2,457,204.439583	77	−28.640	0.132	−2.398	0.182	−67.966	0.166	41.761	0.206
2,457,205.466712	115	−8.225	0.175	−23.512	0.219	−45.066	0.181	17.131	0.213
2,457,206.404903	148	2.022	0.087	−31.511	0.127	−31.511	0.127	2.022	0.087
2,457,206.508631	141	1.481	0.089	−36.269	0.311	−26.209	0.273	1.481	0.089
2,457,207.415514	106	9.428	0.138	−43.305	0.205	−14.533	0.114	−14.533	0.114
2,457,207.519392	111	9.370	0.144	−44.657	0.213	−14.633	0.106	−14.633	0.106
2,457,207.547575	92	8.936	0.157	−44.974	0.237	−14.606	0.116	−14.606	0.116
2,457,210.467746	115	16.897	0.228	−51.306	0.227	5.854	0.258	−35.446	0.227
2,457,210.496392	99	16.690	0.224	−51.347	0.230	5.724	0.261	−35.509	0.223
2,457,234.396006	87	−15.123	0.052	−15.123	0.052	−15.123	0.052	−15.123	0.052
2,457,235.417500	87	−36.495	0.289	4.618	0.239	−51.053	0.289	23.735	0.236
2,457,236.407512	133	−61.497	0.098	31.786	0.117	−83.062	0.086	57.428	0.113
2,457,237.460821	138	−88.241	0.105	59.267	0.168	−70.586	0.117	43.846	0.173
2,457,238.422082	105	−87.637	0.210	59.069	0.290	−48.249	0.255	21.223	0.305
2,457,240.529068	80	−26.729	0.965	−1.422	0.402	−13.932	0.295	−13.932	0.295

for an epoch difference of 2–3 yr (see Table 4 for a comparison). Finally, the *Gaia* satellite mission (Eyer et al. 2015), with its 24 μ as astrometric accuracy for $V = 15$ mag stars and spatial resolution of 0.1 mas in scanning direction and 0.3 mas in cross-direction, can resolve the two binaries easily. The nonsingle stars catalog is scheduled to appear in the fourth *Gaia* release at the end of 2018.

This work is based on observations with the 2 m Alfred Jensch Telescope of the Thüringer Landessternwarte Tautenburg. It has made use of data collected by the *Kepler* satellite mission, which is funded by the NASA Science Mission directorate. Some of the data presented herein were obtained at the W. M. Keck Observatory, which is operated as a scientific partnership among the California Institute of Technology, the University of California, and the National Aeronautics and Space Administration. The observatory was made possible by the generous financial support of the W. M. Keck Foundation. This work has made use of the VALD database, operated at Uppsala University, the Institute of Astronomy RAS in Moscow, and the University of Vienna. The project has been supported by the Hungarian OTKA Grant K113117.

APPENDIX A SPECTROSCOPIC FLUX RATIOS FROM THE DECOMPOSED SPECTRA OF MULTIPLE SYSTEMS

Let I be the observed, composite spectrum showing the lines of n stars, normalized to the total continuum of all n stars, and I_k , $k = 1..n$, the decomposed spectra of the single stars

normalized to the same total continuum,

$$I = \sum_{k=1}^n I_k - (n - 1) \quad (12)$$

or, in line depths with $i = 1 - I$,

$$i = \sum_{k=1}^n i_k. \quad (13)$$

The decomposed spectra shall be fitted by the synthetic spectra S_k , which are normalized to the individual continua of the single stars. In the ideal case we have $i_k = f_k s_k$, where $s_k = 1 - S_k$ are the line depths of the synthetic spectra, f_k is the flux ratio of star k compared to the total continuum flux, and $\sum f_k = 1$. In the following we consider the simplest case of constant f_k (the derivation can easily be extended to wavelength-dependent f_k by developing $f_k(\lambda)$ into a polynomial in wavelength λ). We define

$$\chi^2 = \sqrt{\sum_{\lambda} \sum_{k=1}^n \frac{(i_k - f_k s_k)^2}{\sigma_k^2}}, \quad (14)$$

where σ_k is a weighting factor corresponding to the mean uncertainty of the observed spectrum i_k . Setting

$$f_1 = 1 - \sum_{j=2}^n f_j, \quad (15)$$

we minimize

$$\sum_{\lambda} \left(\frac{1}{\sigma_1^2} \left[i_1 - \left(1 - \sum_{j=2}^n f_j \right) s_1 \right]^2 + \sum_{k=2}^n \frac{(i_k - f_k s_k)^2}{\sigma_k^2} \right). \quad (16)$$

Setting the partial derivatives of Equation (16) with respect to f_2 to f_n to zero yields, with $k = 2..n$,

$$\sum_{\lambda} \left(\frac{s_1}{\sigma_1^2} \left[i_1 - \left(1 - \sum_{j=2}^n f_j \right) s_1 \right] - \frac{s_k}{\sigma_k^2} (i_k - f_k s_k) \right) = 0. \quad (17)$$

Sorting by the f_k and dividing by $[s_1^2]/\sigma_1^2$, we obtain, with $k = 2..n$,

$$\frac{\sigma_1^2 [s_k^2]}{\sigma_k^2 [s_1^2]} f_k + \sum_{j=2}^n f_j = 1 + \frac{\sigma_1^2 [s_k i_k] - \sigma_k^2 [s_1 i_1]}{\sigma_k^2 [s_1^2]}, \quad (18)$$

where the brackets mean the sum over all wavelength bins. Equation (18) is equivalent to the system of linear equations

$$\begin{aligned} a_2 f_2 + f_3 + \dots + f_n &= h_2 \\ f_2 + a_3 f_3 + \dots + f_n &= h_3 \\ &\vdots \\ f_2 + f_3 + \dots + a_n f_n &= h_n \end{aligned} \quad (19)$$

with

$$a_k = 1 + \frac{\sigma_1^2 [s_k^2]}{\sigma_k^2 [s_1^2]} \quad (20)$$

$$h_k = 1 + \frac{\sigma_1^2 [s_k i_k] - \sigma_k^2 [s_1 i_1]}{\sigma_k^2 [s_1^2]}. \quad (21)$$

The flux ratios follow from solving Equation (19). Doing this using a grid of atmospheric parameters p_k to calculate different synthetic spectra $s_k(p_k)$ finally yields the optimum set of atmospheric parameters, together with the corresponding optimum flux ratios.

APPENDIX B MEASURED RVs

Table 5 lists the date of mean exposure, the signal-to-noise ratio of the spectra, and the RVs of the four components of KIC 7177553 plus their errors in km s^{-1} , measured from multi-Gaussian fits to the LSD profiles.

REFERENCES

- Aerts, C. 2015, *AN*, **336**, 477
- Armstrong, D. J., Gómez Maqueo Chew, Y., Faedi, F., & Pollacco, D. 2014, *MNRAS*, **437**, 3473
- Borkovits, T., Derekas, A., Fuller, J., et al. 2014, *MNRAS*, **443**, 3068
- Borkovits, T., Derekas, A., Kiss, L. L., et al. 2013, *MNRAS*, **428**, 1656
- Borkovits, T., Hajdu, T., Sztakovics, J., et al. 2015, arXiv:1510.08272 (B15)
- Borucki, W. J., Koch, D. G., Basri, G., et al. 2011, *ApJ*, **728**, 117
- Bowler, B. P., Liu, M. C., Shkolnik, E. L., & Tamura, M. 2015, *ApJS*, **216**, 7
- Brown, T. M., Gilliland, R. L., Noyes, R. W., & Ramsey, L. W. 1991, *ApJ*, **368**, 599
- Campante, T. L., Chaplin, W. J., Lund, M. N., et al. 2014, *ApJ*, **783**, 123
- Carter, J. A., Fabrycky, D. C., Ragozzine, D., et al. 2011a, *Sci*, **331**, 562
- Carter, J. A., Rappaport, S., & Fabrycky, D. 2011b, *ApJ*, **728**, 139
- Castelli, F., & Kurucz, R. L. 2004, arXiv:astro-ph/0405087
- Chaplin, W. J., Kjeldsen, H., Bedding, T. R., et al. 2011, *ApJ*, **732**, 54
- Chaplin, W. J., & Miglio, A. 2013, *ARA&A*, **51**, 353
- Claret, A., & Gimenez, A. 1993, *A&A*, **277**, 487
- Cox, A. N. 2000, *Allen's Astrophysical Quantities* (4th ed.; New York: Springer)
- Derekas, A., Kiss, L. L., Borkovits, T., et al. 2011, *Sci*, **332**, 216
- Di Folco, E., Dutrey, A., Guilloteau, S., et al. 2014, in SF2A-2014: Proc. Annual Meeting of the French Society of Astronomy and Astrophysics, ed. J. Ballet et al., 135
- Donati, J.-F., Semel, M., Carter, B. D., Rees, D. E., & Collier Cameron, A. 1997, *MNRAS*, **291**, 658
- Everett, M. E., Howell, S. B., & Kinemuchi, K. 2012, *PASP*, **124**, 316
- Eyer, L., Rimoldini, L., Holl, B., et al. 2015, in ASP Conf. Ser. 496, *Living Together: Planets, Host Stars and Binaries*, ed. S. M. Rucinski, G. Torres, & M. Zejda (San Francisco, CA: ASP), 121
- Fuller, J., Derekas, A., Borkovits, T., et al. 2013, *MNRAS*, **429**, 2425
- Gilliland, R. L., Jenkins, J. M., Borucki, W. J., et al. 2010, *ApJL*, **713**, L160
- Greiss, S., Steeghs, D., Gänsicke, B. T., et al. 2012, *AJ*, **144**, 24
- Hadrava, P. 1995, *A&AS*, **114**, 393
- Hadrava, P. 2006, *Ap&SS*, **304**, 337
- Høg, E., Fabricius, C., Makarov, V. V., et al. 2000, *A&A*, **355**, L27
- Klinglesmith, D. A., & Sobieski, S. 1970, *AJ*, **75**, 175
- Kupka, F. G., Ryabchikova, T. A., Piskunov, N. E., Stempels, H. C., & Weiss, W. W. 2000, *BaltA*, **9**, 590
- Lehmann, A., Tkachenko, A., Semaan, T., et al. 2011, *A&A*, **526**, A124
- Lehmann, H., Zechmeister, M., Dreizler, S., Schuh, S., & Kanzler, R. 2012, *A&A*, **541**, A105
- Lenz, P., & Breger, M. 2005, *CoAst*, **146**, 53
- Matijević, G., Prša, A., Orosz, J. A., et al. 2012, *AJ*, **143**, 123
- Ngo, H., Knutson, H. A., Hinkley, S., et al. 2015, *ApJ*, **800**, 138
- Pavlovski, K., & Hensberge, H. 2010, in ASP Conf. Ser. 435, *Binaries—Key to Comprehension of the Universe*, ed. A. Prša, & M. Zejda (San Francisco, CA: ASP), 207
- Prša, A., Batalha, N., Slawson, R. W., et al. 2011, *AJ*, **141**, 83
- Prša, A., Matijević, G., Latkovic, O., Vilardell, F., & Wils, P. 2011, *Astrophysics Source Code Library*, ascl:1106.002
- Prša, A., & Zwitter, T. 2005, *ApJ*, **628**, 426
- Rauer, H., Catala, C., Aerts, C., et al. 2014, *ExA*, **38**, 249
- Reipurth, B., Clarke, C. J., Boss, A. P., et al. 2014, in *Protostars and Planets VI*, ed. H. Beuther et al. (Tucson, AZ: Univ. Arizona Press), 267
- Schlesinger, F. 1910, *PALIO*, **1**, 33
- Shulyak, D., Tsymbal, V., Ryabchikova, T., Stütz, C., & Weiss, W. W. 2004, *A&A*, **428**, 993
- Škoda, P., & Hadrava, P. 2010, in ASP Conf. Ser. 435, *Binaries—Key to Comprehension of the Universe*, ed. A. Prša, & M. Zejda (San Francisco, CA: ASP), 71
- Skrutskie, M. F., Cutri, R. M., Stiening, R., et al. 2006, *AJ*, **131**, 1163
- Slawson, R. W., Prša, A., Welsh, W. F., et al. 2011, *AJ*, **142**, 160
- Tenenbaum, P., Christiansen, J. L., Jenkins, J. M., et al. 2012, *ApJS*, **199**, 24
- Tkachenko, A. 2015, *A&A*, **581**, A129
- Tkachenko, A., Van Reeth, T., Tsymbal, V., et al. 2013, *A&A*, **560**, A37
- Tsymbal, V. 1996, in ASP Conf. Ser. 108, *M.A.S.S., Model Atmospheres and Spectrum Synthesis*, ed. S. J. Adelman, F. Kupka, & W. W. Weiss (San Francisco, CA: ASP), 198
- Welsh, W. F., Orosz, J. A., Aerts, C., et al. 2011, *ApJS*, **197**, 4
- White, T. R., Bedding, T. R., Stello, D., et al. 2011, *ApJL*, **742**, L3
- Yelda, S., Lu, J. R., Ghez, A. M., et al. 2010, *ApJ*, **725**, 331